Journal of
Synchrotron Radiation

ISSN 0909-0495

Received 22 June 2009
Accepted 20 November 2009

X-ray spectromicroscopy in soil and environmental sciences

J. Thieme,[a]* J. Sedlmair,[b] S.-C. Gleber,[b] J. Prietzel,[c] J. Coates,[d] K. Eusterhues,[e] G. Abbt-Braun[f] and M. Salome[g]

[a]Brookhaven National Laboratory, NSLS-II Project, Building 817, Upton, NY 11973, USA, [b]University of Göttingen, Institute for X-ray Physics, Friedrich-Hund-Platz 1, 37077 Göttingen, Germany, [c]Technische Universität München, Chair for Soil Science, 85350 Freising-Weihenstephan, Germany, [d]University of California Berkeley, Department of Plant and Microbial Biology, 271 Koshland Hall, Berkeley, CA 94720, USA, [e]University of Jena, Institute for Geosciences, Burgweg 11, 07749 Jena, Germany, [f]Universität Karlsruhe, Chair for Water Chemistry, Engler-Bunte-Ring 1, 76131 Karlsruhe, Germany, and [g]European Synchrotron Radiation Facility, 6 Rue Jules Horowitz, 38043 Grenoble Cedex, France. E-mail: jthieme@bnl.gov

X-ray microscopy is capable of imaging particles in the nanometer size range directly with sub-micrometer spatial resolution and can be combined with high spectral resolution for spectromicroscopy studies. Two types of microscopes are common in X-ray microscopy: the transmission X-ray microscope and the scanning transmission X-ray microscope; their set-ups are explained in this paper. While the former takes high-resolution images from an object with exposure times of seconds or faster, the latter is very well suited as an analytical instrument for spectromicroscopy. The morphology of clusters or particles from soil and sediment samples has been visualized using a transmission X-ray microscope. Images are shown from a cryo-tomography experiment based on X-ray microscopy images to obtain information about the three-dimensional structure of clusters of humic substances. The analysis of a stack of images taken with a scanning transmission X-ray microscope to combine morphology and chemistry within a soil sample is shown. X-ray fluorescence is a method ideally applicable to the study of elemental distributions and binding states of elements even on a trace level using X-ray energies above 1 keV.

© 2010 International Union of Crystallography
Printed in Singapore – all rights reserved

Keywords: X-ray microscopy; spectromicroscopy; XANES; NEXAFS; environmental sciences; colloids; nanoparticles.

1. The benefits of X-ray spectromicroscopy for geo- and environmental sciences

Environmental science is a widespread research area influenced by the need to understand many different chemical and physical processes. Owing to this complexity of environmental processes and the many mutual interactions involved, competence is required in more than one area of expertise and a multidisciplinary approach to address open scientific issues is often necessary. Geochemistry, hydrology, microbiology, atmospheric science and soil science, to name a few, are essential scientific fields in this regard. For example, the complex roles of carbon, nitrogen, phosphorus and sulfur cycles in the environment are still incompletely understood as are their mutual interactions. Similarly, our knowledge of uptake and metabolism of environmental contaminants by biological organisms is far from complete. Elemental transport, redox processes, microbial activity and anthropogenic influences all affect these processes. Knowledge of each individual piece of the puzzle contributes to a better understanding of the overall picture.

X-ray spectromicroscopy is a very useful tool for environmental sciences owing to its high spectral and spatial resolution. In the areas of material science, biology and medical sciences it has already been used successfully. Now it is starting to be used in environmental studies, for example in the form of spectromicroscopy with a spatial resolution below 50 nm in the sub-keV X-ray energy range and in the form of X-ray fluorescence studies in the keV energy range with a spatial resolution below 100 nm (Aoki *et al.*, 2006; Susini *et al.*, 2003). The combination of high-resolution microscopy with spectroscopic capabilities allows for the determination of elemental compositions as well as for chemical speciation and the identification of trace elements on length scales extending to the nanoscale.

For the understanding of many processes in the environment it is crucial to not only consider the submicrometer world accessible by spectromicroscopy. Heterogeneity exists in the

environment over a wide range of length scales. Therefore, good data have to be available for statistics and for the developments of models. It is also necessary to connect the achieved results to standard measurements in other as well as similar systems. The phosphorus depletion or enhancement in agricultural soils is one example (Lombi *et al.*, 2006). Environmental sciences strongly interact with biology, *e.g.* in the study of biofilms, or of biogeochemical pathways in environmental problems. Biological and microbial processes are crucial within environmental science. Therefore, an integrated approach is essential for studying biological as well as other aspects of environmental problems.

Metals and metalloids constitute a core interest in the field of geo- and environmental sciences. Iron is one of the most ubiquitous elements at the earth's surface and of particular interest as it forms very reactive, often nanomete-sized, Fe(III) oxyhydroxides in soils and sediments. Even if present at a low concentration, they may control the adsorption, *i.e.* the mobility and bioavailability of many nutrients, pollutants and organic molecules. Under reducing conditions the oxyhydroxides transform into Fe(II) minerals, so that past redox processes can often be traced back by analyzing the Fe oxidation state of fine-grained Fe minerals. X-ray absorption near-edge spectroscopy (XANES) has been proven to be a well suited tool for this task (LaForce & Fendorf, 2000; Wilke *et al.*, 2001; O'Day *et al.*, 2004; Prietzel, Thieme, Eusterhues & Eichert, 2007). Spatially resolved sulfur and phosphorus speciation is important to a wide range of issues, *e.g.* iron and copper oxidation in soils. The role of phosphorus in marine systems has been studied with spatially resolved XANES showing the importance of these processes to this environment (Brandes *et al.*, 2007). Halogenous compounds, *e.g.* the chlorine speciation in plants, or the relation of chlorine to organic compounds and iron have successfully be determined by Leri *et al.* (2006). Fluorine and bromine occur in much lower concentrations in the environment. To be analyzed, an exceptional sensitivity of the method is needed, a strong argument for X-ray fluorescence studies.

Altogether, X-ray spectromicroscopy has the unique capability of quantitative chemical analysis on a molecular and not just elemental basis, with a quantization based on high-resolution X-ray absorption or photoelectron spectroscopy. It can be applied to complex materials including buried interfaces, poorly crystalline or even amorphous phases, wet samples (*e.g.* biological and environmental) and vacuum- and radiation-sensitive materials. By combining spectroscopic chemical information with high spatial resolution, X-ray spectromicroscopy provides many new research opportunities.

Using synchrotron radiation as a light source, the incident X-ray energy is tunable, a mandatory precondition for spectromicroscopy. The spatial resolution achieved by the existing spectromicroscopy stations is below 100 nm, which is crucial for XANES studies of colloids or nanoparticles. The available instrumentation performs fast wide-range scans as well as slower high-resolution scans to obtain overview maps of a sample as well as zooming into a detailed area of interest for studies with utmost resolution. Tomographic studies of systems from geosciences and environment sciences can be realised, *e.g.* to understand transport processes. The availability of the X-ray energy range of the so-called water window between E = 0.25 keV and E = 530 eV, and of X-ray energies above E = 1 keV, especially up to approximately E = 25 keV, ensures that a very large part of the current research interests can be addressed.

2. X-ray spectromicroscopy in the water window

In 1952 Horst Wolter wrote that X-radiation in the energy range between the *K*-absorption edge of carbon and of oxygen is very well suited for microscopy purposes. For this energy range he created the phrase 'water window' (Wolter, 1952). The reason for this name-giving becomes clear when looking at the linear absorption coefficients plotted in Fig. 1.

The intensity I_1 of X-rays transmitted through an object can be calculated using the Lambert–Beer equation (Attwood, 2000), $I_1 = I_0 \exp(-\mu_1 d)$. Here I_0 is the incident radiation, μ_1 is the linear absorption coefficient, and d is the thickness of the object along the path of the X-rays. A good measure for calculating the penetration of X-rays through a sample is to determine at what thickness the transmitted radiation I_1 is weakened to $1/e$ of the incident intensity I_0. The resulting penetration depth $1/\mu_1$ for water ranges from 2 µm at the carbon *K*-edge up to 10 µm at the oxygen *K*-edge. In contrast, the intensity of 150 keV electrons is reduced to this value at a sample thickness of only 0.2 µm. This means that much thicker samples can be investigated using X-ray microscopy (Kirz *et al.*, 1995).

In Fig. 1 the linear absorption coefficients μ_1 of water, of the mineral smectite and of the organic molecule phenol are plotted as a function of the incident X-ray energy. Smectite is a clay mineral abundant in soils and sediments while phenolic

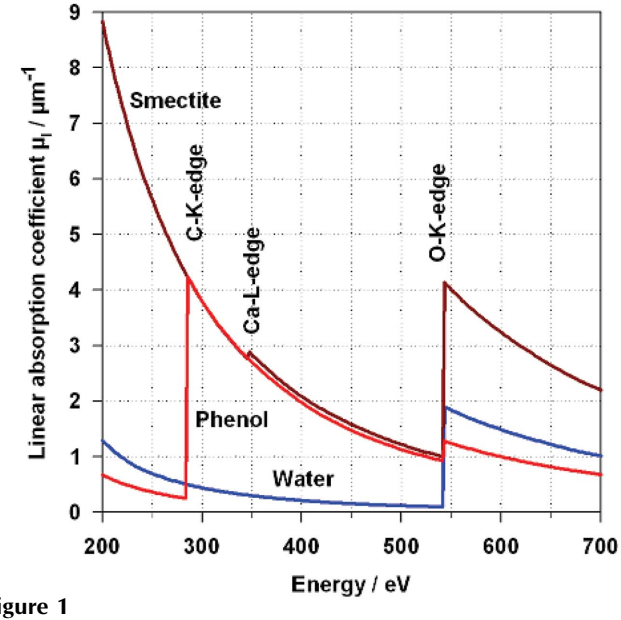

Figure 1
Linear absorption cross section μ_1 of a clay mineral (smectite), an organic molecule (phenol) and of water as a function of X-ray energy. The absorption edges of oxygen, calcium and carbon are marked.

compounds can be found in a large set of natural organic materials. Both substances can be understood as representatives of inorganic or organic matter. The linear absorption coefficient μ_1 of water, compared with that of organic or inorganic matter between the *K*-absorption edge of carbon and of oxygen, is significantly lower. This absorption difference gives rise to the natural amplitude contrast when imaging a specimen with X-rays within this energy range. As a result, samples can be studied directly in aqueous media without fixation or staining.

The spatial resolution achievable when looking at a sample using a microscope is directly related to the energy of the radiation. Increasing the energy implies increasing the resolution capabilities, *i.e.* the higher the energy the smaller the structures visible. Compared with visible light, the energy of the X-rays used for experiments in the water window is much higher. This means that with an X-ray microscope a much better resolution can be achieved than with a conventional microscope using visible light. At present, the smallest structures visible with an X-ray microscope are less than 15 nm in size (Chao *et al.*, 2005).

In the X-ray energy region of the water window the complex refractive index is $n = 1 - \delta - i\beta$. The values for δ and β are very small leading to a refractive index very close to unity (Henke *et al.*, 1993). Therefore, scattered X-ray light will not be reflected from inner surfaces in inhomogeneous media (Pohl, 1967). Although there is a huge difference between the lateral resolution and the penetration depth, clear images can be expected even when studying thick and heterogeneous specimens.

A light source usable for spectromicroscopy experiments has to be highly brilliant and must supply radiation over a wide energy range. Up to now, only electron storage rings, *i.e.* large-scale facilities providing synchrotron radiation, are capable of meeting these needs. Therefore, all spectromicroscopy stations are set up at these light sources. With a monochromator it is possible to reduce the bandwidth of the radiation to a very small value and thus to tune the energy of the X-radiation impinging on the sample in very fine steps. This allows for mapping elements and for the determination of binding states. For obtaining a distribution map of a single element within a sample it is sufficient to take two images with X-ray energies above and below the absorption edge of this element. Dividing the spatial-resolved absorption values at each point gives rise to a distribution of this element in the sample.

To examine binding states of the chemical elements within a sample, near-edge resonances for XANES studies can be used (Stöhr, 1992). When the used X-ray energy is tuned across the absorption edge, resonances appear reflecting the chemical bonding state of the element. These resonances superimpose the step-like rise in absorption owing to the element. Important absorption edges within the energy range of the water window are listed in Table 1. Knowing the intensity I_0 impinging on the sample and measuring the intensity I transmitted through the sample, spectra can be created showing the optical density ($\mu_1 d$) as a function of the X-ray energy. From these spectra the binding states within the sample can be derived.

Table 1
K- and *L*-absorption edges within the energy range of the water window.

Element	Edge	Energy (eV)
Carbon	*K*	284
Potassium	L_2, L_3	297, 295
Calcium	L_2, L_3	350, 346
Nitrogen	*K*	410
Oxygen	*K*	534

In summary, X-ray microscopy in the water window is a tool capable of imaging particles in the nanometer size range directly in their aqueous environment with high spatial resolution, and furthermore it is possible to combine this with high spectral resolution for spectromicroscopy studies.

Fresnel zone plates, *i.e.* circular diffraction gratings with a decreasing line width while increasing their radius, work with X-rays like thin lenses in visible light. They are commonly used as high-resolution optical elements in X-ray microscopy, both in a transmission X-ray microscope and in a scanning transmission X-ray microscope (Schmahl & Rudolph, 1969).

The optical set-up of a transmission X-ray microscope is very similar to a conventional light microscope. It consists of a monochromator, a condenser and a micro zone plate. The monochromator reduces the bandwidth of the synchrotron radiation coming from the electron storage ring to a $E/\Delta E$ value of several hundred up to several thousand. This reduction of the bandwidth is necessary, as the micro zone plate only acts as a high-resolution optical element when supplied with quasi-monochromatic radiation. The condenser focuses the radiation onto the object. The micro zone plate is placed downstream of the object. It creates an enlarged image of the object in the image plane, which is recorded by a CCD camera using exposure times in the range of seconds and below. The X-ray images presented here have been taken with the X-ray microscope designed by the Institute for X-ray Physics in the University of Göttingen and operated with the undulator U41 at the electron storage ring BESSY II in Berlin (Guttmann *et al.*, 2003). The X-radiation coming from the undulator U41 is reduced in bandwidth and focused onto the object by an off-axis transmission zone plate. A mirror set, consisting of one fixed and two rotating mirrors, provides for aperture matching with the micro zone plate and for incoherent illumination of the sample. Using this rotating mirror condenser the bandwidth reduction of the radiation is $E/\Delta E = 2000$, leading to a very high clarity of the images (Niemann *et al.*, 2003). A back-illuminated thinned CCD camera records the image generated by the micro zone plate. A new instrument has been recently set up at BESSY II by Schneider *et al.* (2007). Further transmission X-ray microscopes are also operated at the Advanced Light Source, Berkeley, USA (Fischer *et al.*, 2006; Meyer-Ilse *et al.*, 2000), the storage ring Astrid in Arhus, Denmark (Medenwaldt & Uggerhøj, 1998) and in a dual microscopy set-up (TwinMic) at ELETTRA, Trieste, Italy (Kaulich *et al.*, 2003).

Figs. 2 and 3 show examplary X-ray microscopy images of soil and sediment particles in aqueous solutions. The image in Fig. 2 has been recorded within a few seconds exposure time and shows a cluster of colloidal particles from a Chernozem soil. Clay particles are clearly visible, revealing their platelet-like structure. The arrow in the lower left corner of the image indicates a stack of platelets aligned with their surface along the path of the X-rays. Therefore, when the absorption is high, the structure appears black. The clay particle indicated with the other arrow labeled 'Clay' has itself oriented perpendicular to the beam. As these platelets are very thin, the absorption is not that high, and the particle appears at a certain gray level. Bacteria are visible in this image as dense round or ellipsoidal lines, as can be seen at the tip of the arrow labeled 'Bact'. Here, the cell wall with its high organic content in comparison with the inner structure of the cell absorbs stronger the penetrating X-rays. Fig. 3 shows an X-ray microscopy image composed of ten single images, showing an association of colloidal particles found in the sediment of Hamburg harbor. A long chain of bacteria is visible, indicated by the arrow labeled 'Bact', and a large diatom skeleton, also indicated by an arrow. These composed images show that although the X-ray microscope has a limited field of view it is possible to depict large structures. Both images have been taken with an optical set-up achieving ~30 nm spatial resolution

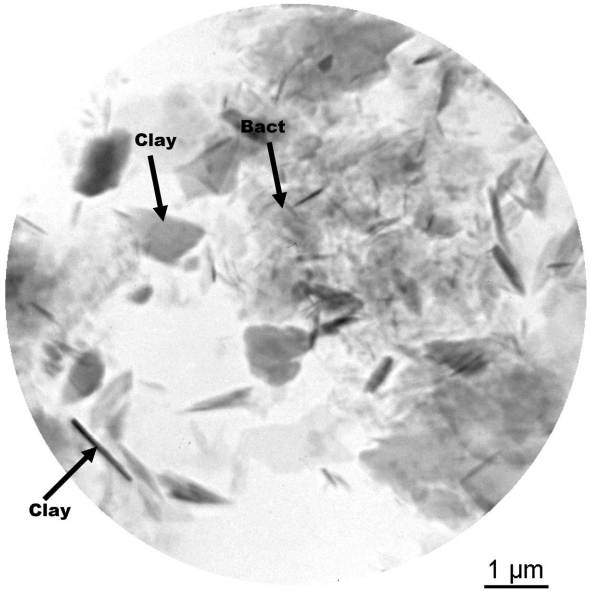

Figure 2
Transmission X-ray microscopy image of an association of soil colloids in aqueous dispersion, taken at $E = 520$ eV with the TXM at BESSY, Berlin. Clay platelets and bacteria are indicated by arrows.

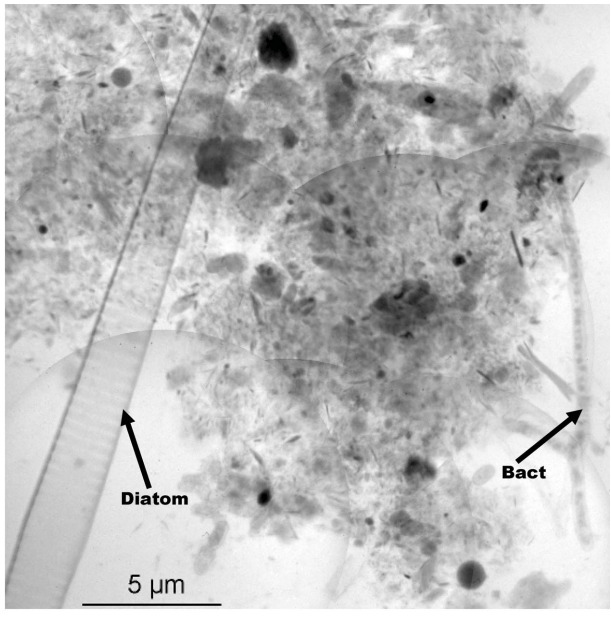

Figure 3
Composite transmission X-ray microscopy image of an association of colloidal particles from Hamburg harbor sediments in aqueous dispersion, taken at $E = 520$ eV with the TXM at BESSY, Berlin. Bacteria and a diatom skeleton are indicated by arrows.

X-ray microscopy images are usually two-dimensional projections; therefore it is not possible to clarify an exact spatial arrangement of colloidal structures. All particles are clearly visible, but the question remains as to whether they are attached to each other or whether there is a distance between them not visible in that particular projection. Distances between particles along the optical path cannot be revealed by these images. X-ray stereo microscopy can probe the proximity relation between particles with just two images (Gleber *et al.*, 2009). Tomography based on X-ray microscopy images reveals the complete three-dimensional morphology of the sample. The transmission X-ray microscope of the Center for X-ray Optics at beamline 6.1.2 of the Advanced Light Source, Lawrence Berkeley Laboratory, Berkeley, has been used successfully for such experiments (Thieme *et al.*, 2003). This can be seen in the following example. To obtain information about the morphological changes of clusters of humic substances undergoing redox change, the three-dimensional structure has been imaged with cryo-tomography based on X-ray microscopy images. Capillaries with diameters of ~8–10 µm were used to hold the samples, subsequently shock-frozen and kept at liquid-nitrogen temperatures to prevent changes in the sample owing to radiation damage during recording of the tomography data set. The sample here has been a microbially reduced humic substance from Suwannee River, a well characterized humic substance from the International Humic Substances Society. Simply exposing the test tube to air has reoxidized the reduced sample. In Fig. 4 two images of the computer reconstruction of the three-dimensional structure calculated from this data set reveal the changes in the spatial arrangement of the humic substances. The resolution of the tomographic data set has been determined to be 45 nm. Using tomography it can be verified that humic substances, appearing as a sponge-like structure in a reduced state, change dramatically their morphology to isolated clusters when reoxidized (Coates *et al.*, 2000; Thieme *et al.*, 2007). A new approach for relatively flat and extended samples has been accomplished with success recently, leaning on experiences from electron tomography (Heim *et al.*, 2009).

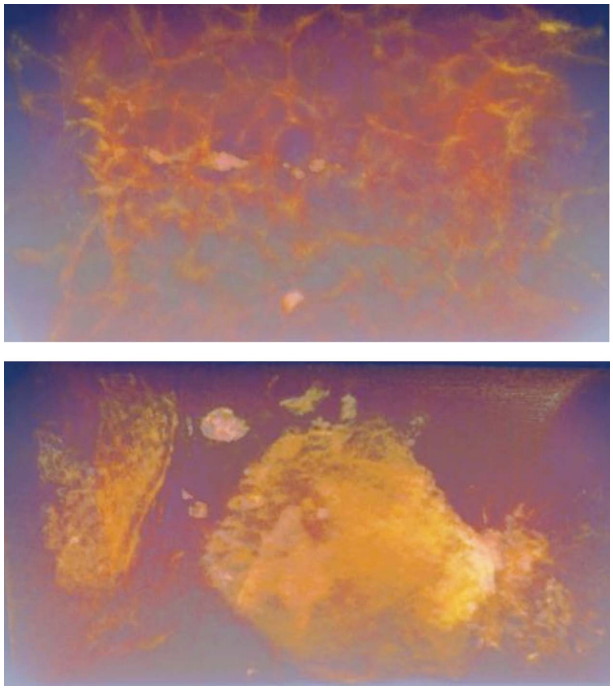

Figure 4
Tomographic reconstruction of the morphology of clusters of humic substances in a reduced (top image) and a re-oxidized (bottom image) state. The samples were filled into capillaries with diameters of 8 μm (top) and 10 μm (bottom) and kept at cryogenic temperatures. The glass walls are the top and the bottom limits of the images. The change in morphology as a result of the redox change is obvious.

For a scanning transmission X-ray microscope the bandwidth of the polychromatic synchrotron radiation is reduced by a grating monochromator to a $E/\Delta E$ value of several thousands. The micro zone plate focuses this radiation into a spot of diffraction-limited size onto the sample. A detector records the radiation transmitted through the object and the signal is stored on computer. By scanning either the focus spot over the sample or the sample across this spot and recording the transmitted signal as a function of the scan position, an image can be generated in the computer. Owing to the scanning process, the total time needed for the generation of an image is longer than that using a transmission X-ray microscope. Tuning the energy of the X-radiation with the monochromator and keeping the position of the light spot on the sample, a spectrum can be measured from this specific object point. By using a segmented detector it is possible to detect the signal not only in bright-field mode but also in dark-field and in differential-phase contrast mode simultaneously. The examplary results presented here have been taken with the scanning transmission X-ray microscope, designed by the Institute for X-ray Physics in the University of Göttingen (Wiesemann *et al.*, 2003; Mitrea *et al.*, 2008). The monochromator consists of a plane mirror and a plane grating with variable line density (Wiesemann *et al.*, 2001). The latter provides for reduction of the bandwidth of the radiation and for a coherent illumination of the micro zone plate. Thus, the zone plate creates the desired diffraction-limited small spot. The zone plate, and so the focal spot, is moved by a piezo scanning device with an accuracy of a few nanometers across the sample. To choose beforehand regions of interest, the sample can be looked at using a visible-light microscope, which also allows for pre-focusing. Subsequently, the sample can be scanned coarsely by using stepper motors for gaining a more detailed overview. A pn-CCD camera behind the object acts as a configured detector. Additional scanning transmission X-ray microscopes for the energy range discussed here are set up at the electron storage rings NSLS (Jacobsen *et al.*, 1991) and ALS (Warwick *et al.*, 1998; Ade *et al.*, 2003) in the USA, the Canadian Light Source (Kaznatcheev *et al.*, 2007) and the Swiss Light Source (Flechsig *et al.*, 2006).

Typically, transmission X-ray microscopes are used to take high-resolution images of an object with exposure times of a few seconds or less, whereas the slower scanning transmission X-ray microscope is an ideal instrument for spectromicroscopy studies. An intrinsic advantage of a scanning transmission X-ray microscope is that the micro zone plate is located in front of the sample. Therefore, the detector collects all radiation penetrating the sample. Zone plates show diffraction efficiencies of around 10%, meaning that only this part of the radiation is used in a transmission X-ray microscope for image generation. This results in a much lower dose and thus lower radiation damage when studying a sample with a scanning transmission X-ray microscope.

Fig. 5 shows an example of mapping the carbon distribution within an undisturbed forest soil sample. The left-hand image was taken at an X-ray energy of $E = 280$ eV, just below the K-absorption edge of carbon; the right-hand image was taken at $E = 300$ eV, above the absorption edge. The difference is clearly visible. The left-hand image shows a particle from the soil absorbing only little, whereas in the right-hand image it becomes clear owing to the strong absorption that the whole particle is covered with organics, absorbing strongly. Both images are 10 μm × 15 μm in size, with a pixel size of 50 nm, resulting in 200 × 300 pixels, with a dwell time per pixel of 6 ms.

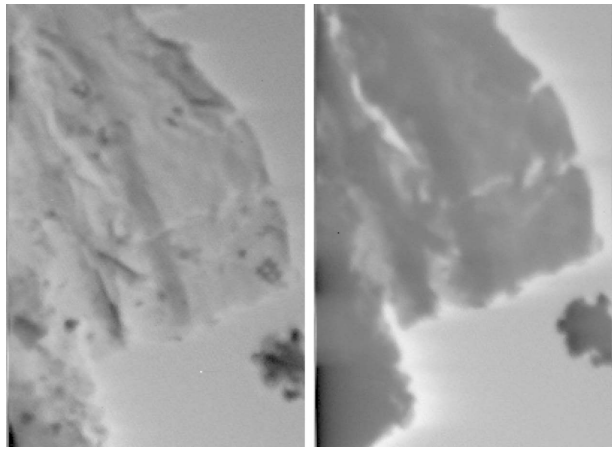

Figure 5
X-ray microscopy images of a colloidal particle from a forest soil, taken at $E = 280$ eV, left, and $E = 300$ eV, right. The difference in absorption owing to crossing the absorption edge is clearly visible. The image size is 10 μm × 15 μm, 200 × 300 pixels, taken with a dwell time per pixel of 6 ms.

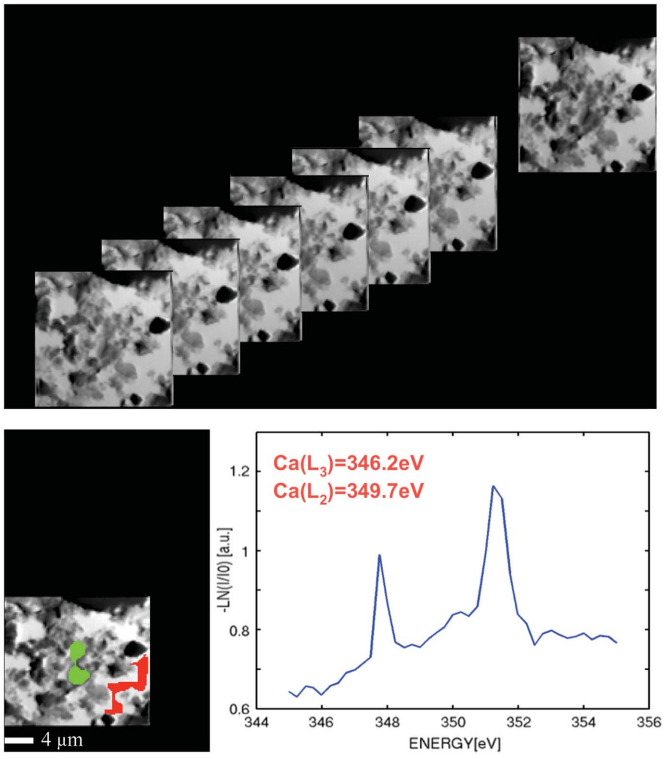

Figure 6
Stack of X-ray images spanning a small energy range across the *L*-absorption edge of calcium of a clay/humic substance dispersion. The lower left picture indicates the areas chosen for obtaining the spectrum at the lower right side. The image size is 20 µm × 20 µm, 100 × 100 pixels, taken with a dwell time per pixel of 6 ms. 40 images with an energy step size of ΔE = 0.25 eV have been taken for this image stack.

To combine spatial information with knowledge of the chemical composition within the sample, a very useful method is to take a stack of images at closely spaced energies throughout the region of interest across the absorption edge of the desired element (Jacobsen *et al.*, 2000). This approach is visualized in Fig. 6, where some images of such a stack from a mixture of a clay with humic substances, taken with the scanning transmission X-ray microscope at BESSY II around the *K*-absorption edge of calcium, are shown. The full set spans a three-dimensional coordinate system of *x*, *y* and the energy. The energy ranges here from E = 345 eV to E = 355 eV with steps of 0.25 eV. The image size is 20 µm × 20 µm with 100 × 100 pixels, a rather moderate resolution, and a dwell time per pixel of 6 ms. Possible drifts and movements within the instrumentation during recording require an alignment of the images to each other afterwards. A spectrum can be obtained by selecting an object region and plotting the optical density of that region as a function of energy. Spectra can be obtained from discrete image pixels as well as from larger regions by integrating the optical density of all pixels within the chosen area. This experiment is more time-consuming than simply taking a spectrum from a fixed position, but spatially and spectrally resolved data of an object are available at the same time. This is demonstrated in the lower part of Fig. 6. On the left-hand side the area of interest within the image is marked in green, the region necessary for I_0 is marked in red. The spectrum shows the optical density, $-\ln(I_1/I_0) = \mu_1 d$. The L_2- and the L_3-peak of calcium are clearly visible, proving that the area marked in green shows a high calcium content. A differentiation of clay and organic substance is hence possible. Therefore, such a spectromicroscopy study provides information about the chemistry within a sample in combination with high spatial resolution. The radiation dose applied to a single point within the sample is the same for point spectra as for stacks.

Table 2
Highly relevant absorption edges in the energy range E = 2–25 keV.

Element	Edge	Energy (eV)
Phosphorus	*K*	2149
Sulfur	*K*	2472
Silver	L_2, L_3	3524, 3351
Cadmium	L_2, L_3	3727, 3537
Calcium	*K*	4038
Iron	*K*	7112
Zinc	*K*	9659
Arsenic	*K*	11868
Lead	L_2, L_3	15198, 13035
Uranium	L_2, L_3	20947, 17167

3. Spectromicroscopy at higher X-ray energies

Scanning fluorescence X-ray microscopes, operating in the X-ray energy range above E = 1 keV, make use of the very high fluorescence yield at these photon energies, thus having an extremely good elemental and chemical sensitivity. Instruments using zone plates for focusing are available for experiments achieving spatial resolutions in the range 50–200 nm (Thieme *et al.*, 2007). They have also been used for X-ray tomography using absorption contrast (Haddad *et al.*, 1994; Wang *et al.*, 2000) and fluorescence contrast (Sutton *et al.*, 2000). Differential phase contrast and the recently developed coherent diffraction imaging are methods used to obtain spatial information with these micro- and nanoprobe instruments (Wilhein *et al.*, 2001; Quiney *et al.*, 2006; Hornberger *et al.*, 2008). Operating in the energy range E = 2–25 keV, providing at the same time spatial resolutions in the range 50–200 nm in combination with tomography and spectroscopy capabilities, X-ray micro- and nanoprobes are powerful instruments for investigations within the submicrometer world. A large number of *K*-, *L*- and *M*-edges of elements relevant in environmental and geosciences are found in this energy range, allowing for a wide spectrum of experiments. A list with only a few elements is given in Table 2. Examples are the study of defects in buried Cu interconnects in Si-based microelectronic circuit chips (Schneider *et al.*, 2002), the spatially resolved speciation of silicon (Bihannic *et al.*, 2001), of sulfur (Solomon *et al.*, 2005; Prietzel, Thieme, Salome & Knicker, 2007), of iron (Prietzel, Thieme, Eusterhues & Eichert, 2007) in soils, and of the role of polyphosphates in marine sediments (Diaz *et al.*, 2008). Spectromicroscopy stations at the ESRF (Susini *et al.*, 2002), the APS (McNulty *et*

al., 2003), just recently at the Australian Synchrotron and in the future at the storage ring NSLS-II are dedicated instruments operating in the energy region mentioned above. Microprobes for X-ray spectroscopy with spatial resolutions in the range of several micrometers are available for experiments at many electron storage rings too. It would exceed the scope of this manuscript to explain these instruments in detail; therefore the interested scientist is referred to the websites of the according storage rings for details.

Scanning fluorescence X-ray microscopes are ideal tools for mapping and quantifying elemental distributions in samples from the environment or from the geosciences. In such an instrument, monochromatic X-rays with a bandwidth of $\Delta E/E = 5 \times 10^{-4}$ or less are focused to a submicrometer spot on the sample. An energy-dispersive detector collects the characteristic X-ray fluorescence emitted by the sample. The sample is scanned through the focal spot, the signal is recorded as a function of position, thus forming a map of the elemental distribution. Because of the exceptional sensitivity of this technique, trace element quantities down to attogram levels can be mapped. Simultaneously, images can be recorded in transmission in bright-field, dark-field or differential-phase contrast by using configured detectors (Feser *et al.*, 2006). Tuning the energy of the incident X-rays across an absorption edge of interest again yields a spectrum from a specific area of the sample. Fine-tuning the X-ray energy to probe the near-edge structure of elemental resonances allows for the study of the chemical state of elements of interest.

An example of the chemical information that can be obtained by measuring the X-ray fluorescence spectra is given in Fig. 7. The sulfur speciation within four refractory organic substances, three fulvic acids and one humic acid (Frimmel *et al.*, 2002), has been recorded using the station at the ESRF. The spectra have in general the same shape: a rise in absorption at the *K*-absorption edge of sulfur in combination with two prominent peaks close to the edge energy. The peak at lower energies represents reduced sulfur species, mainly sulfide; the right-hand peak shows the abundance of oxidized sulfur species, mainly sulfonate and sulfate. Without going into detail, it becomes quickly clear that the humic acid has more reduced species than the fulvic acids and *vice versa* for the oxidized species. So even without a detailed analysis, such a study leads to information about the chemistry of the fate of the sample.

Fig. 8 shows results achieved when studying the annually laminated sediments of Lake Steisslinger See at the storage ring ESRF. The top-left image is an image taken with an optical microscope, showing the lamination of the sample. This lamination originates from the precipitation of carbonates during summer and early autumn and the sedimentation of clay minerals and organic matter during winter and spring. Such laminae are only preserved when bioturbation is prevented and thus evidence anoxic conditions. Even though, XANES at the sulfur *K*-absorption edge was able to determine a different sulfur species distribution in different laminated sediment sections. The lamination is also reproduced when looking at the sample in the X-ray fluorescence light at E = 2490 eV, just above the *K*-absorption edge of sulfur. Sulfur-rich and sulfur-poor layers alternate. To identify the sulfur

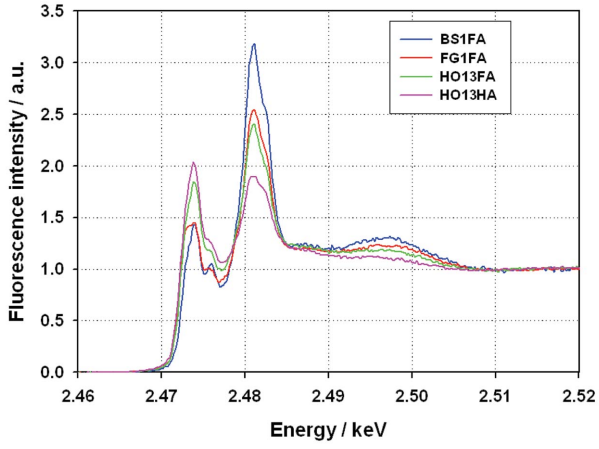

Figure 7
X-ray fluorescence spectra of refractory organic substances from the environment, namely three fulvic acids and one humic acid. The difference in peak height between the fulvic and the humic acids can clearly be seen.

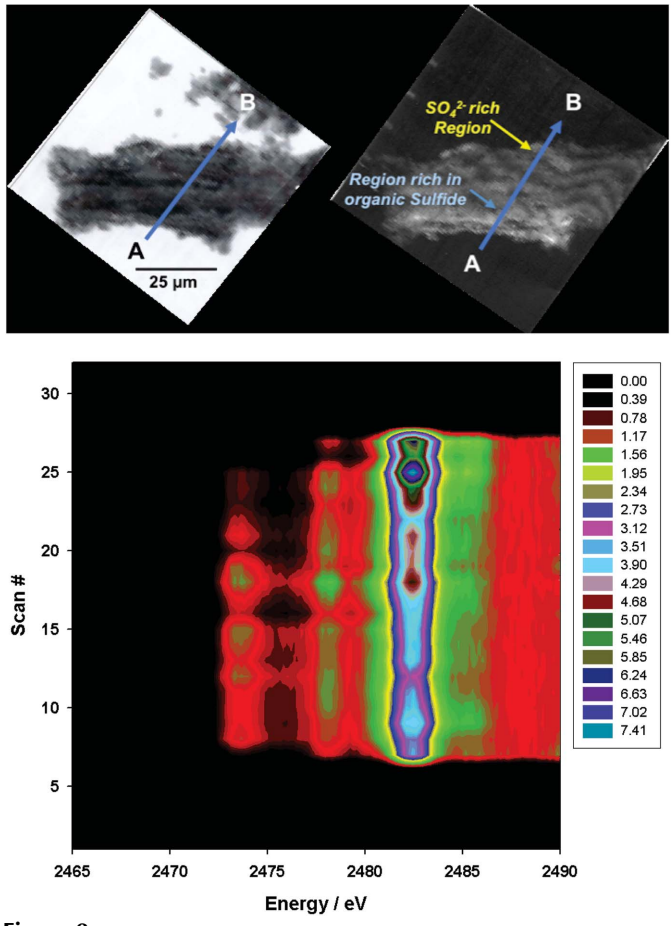

Figure 8
Top left: optical microscope image of a section of a laminated sediment core from the Lake Steisslinger See. Top right: X-ray fluorescence image of the same sediment core taken at E = 2.490 keV, showing the same lamination. Bottom: three-dimensional representation of the XANES spectra across the sediment core, scan numbers increasing from *A* to *B*.

speciation within the layers, a sequence of XANES spectra has been taken, following the trajectory from *A* to *B*, indicated in the top images. The lower image of Fig. 8 is a three-dimensional representation of this set of spectra. It shows that the amount of reduced sulfur species decreases when going from *A* to *B*, whereas the oxidized species become more prominent.

4. Summary

X-ray spectromicroscopy is a tool excellently suited to studying materials from geo- and environmental sciences. It combines high spatial resolution with high spectral resolution, thus connecting morphology with chemistry. Using tomography or the newly developed coherent diffraction imaging, three-dimensional information about the structure of samples on the micro- and nanoscale can be obtained. Unfortunately, only electron storage rings delivering synchrotron radiation are suited as light sources for X-ray spectromicroscopy instruments, limiting the accessibility of these tools for the scientist. As the number of storage rings increases, however, this limitation wanes. With new instruments at newly developed storage rings with increased capabilities, excellent experimental conditions for geo- and environmental experiments can be expected.

The work presented here has been supported by the Federal Minister of Education and Research (BMBF) under contract numbers 05KS1MG1/9 and 02WU9893/0, by the Office of Naval Research under contract number N00014-99-10371, by DFG under contract numbers Th 445/8-1 and Th 445/8-2 and within the SFB755 'Nanoscale Photonic Imaging'. We would like to thank the staff of ALS, ESRF and BESSY II for providing excellent working conditions when performing experiments.

References

Ade, H., Kilcoyne, A., Tyliszczak, T., Hitchcock, P., Anderson, E., Harteneck, B., Rightor, E., Mitchell, G., Hitchcock, A. & Warwick, T. (2003). *J. Phys. IV*, **104**, 3–8.

Aoki, S., Kagoshima, Y. & Suzuki, Y. (2006). Editors. *Proceedings of the 8th International Conference on X-ray Microscopy.* Tokyo: Institute of Pure and Applied Physics Conference Series 7.

Attwood, D. (2000). *Soft X-rays and Extreme Ultraviolett Radiation – Principles and Applications.* Cambridge University Press.

Bihannic, I., Michot, L. J., Lartiges, B. S., Vantelon, D., Labille, J., Thomas, F., Susini, J., Salome, M. & Fayard, B. (2001). *Langmuir*, **17**, 4144.

Brandes, J., Ingall, E. & Paterson, D. (2007). *Mar. Chem.* **103**, 250–265.

Chao, W., Harteneck, B., Liddle, J., Anderson, E. & Attwood, D. (2005). *Nature (London)*, **435**, 1210–1213.

Coates, J., Chakraborty, R., O'Connor, S., Schmidt, C. & Thieme, J. (2000). *Acta Hydrochim. Hydrobiol.* **28**, 420–427.

Diaz, J., Ingall, E., Benitez-Nelson, C., Paterson, D., de Jonge, M. D., McNulty, I. & Brandes, J. (2008). *Science*, **320**, 652–655.

Feser, M., Hornberger, B., Jacobsen, C., De Geronimo, G., Rehak, P., Holl, P. & Strueder, L. (2006). *Nucl. Instrum. Methods Phys. Res. A*, **565**, 841–854.

Fischer, P., Kim, D.-H., Chao, W., Liddle, J. A., Anderson, E. H. & Attwood, D. T. (2006). *Mater. Today*, **9**, 26–33.

Flechsig, U., Quitmann, U., Raabe, J., Böge, M., Fink, R. & Ade, H. (2006). *AIP Conf. Proc.* **879**, 505–508.

Frimmel, F. H., Abbt-Braun, G., Heumann, K. G., Hock, B., Luedemann, H.-D. & Spiteller, M. (2002). Editors. *Refractory Organic Substances in the Environment.* Weinheim: Wiley-VCH.

Gleber, S.-C., Thieme, J., Chao, W. & Fischer, P. (2009). *J. Microsc.* **235**, 199–208.

Guttmann, P., Niemann, B., Rehbein, S., Knöchel, C., Rudolph, D. & Schmahl, G. (2003). *J. Phys. IV*, **104**, 85–90.

Haddad, W. S., McNulty, I., Trebes, J. E., Anderson, E. H., Levesque, R. A. & Yang, L. (1994). *Science*, **266**, 1213–1215.

Heim, E., Guttmann, P., Rehbein, S., Werner, S. & Schneider, G. (2009). *J. Phys. Conf. Ser.* **186**, 012041.

Henke, B., Gullikson, E. & Davis, J. (1993). *Atom. Data Nucl. Data Tables*, **54**, 181–342.

Hornberger, B., de Jonge, M. D., Feser, M., Holl, P., Holzner, C., Jacobsen, C., Legnini, D., Paterson, D., Rehak, P., Strüder, L. & Vogt, S. (2008). *J. Synchrotron Rad.* **15**, 355–362.

Jacobsen, C., Flynn, G., Wirick, S. & Zimba, C. (2000). *J. Microsc.* **197**, 173–184.

Jacobsen, C., Williams, S., Anderson, E., Browne, M., Buckley, C., Kern, D., Kirz, J., Rivers, M. & Zhang, X. (1991). *Opt. Commun.* **86**, 351–364.

Kaulich, B. *et al.* (2003). *J. Phys. IV*, **104**, 103–107.

Kaznatcheev, K., Karunakarana, C., Lanke, U., Urquhart, S., Obst, M. & Hitchcock, A. (2007). *Nucl. Instrum. Methods Phys. Res. A*, **582**, 96–99.

Kirz, J., Jacobsen, C. & Howells, M. (1995). *Q. Rev. Biophys.* **28**, 33–130.

LaForce, M. J. & Fendorf, S. (2000). *Soil Sci. Soc. Am. J.* **64**, 1608–1615.

Leri, A. C., Hay, M. B., Lanzirotti, A., Rao, W. & Myneni, S. C. B. (2006). *Anal. Chem.* **78**, 5711–5718.

Lombi, E., Scheckel, K. G., Armstrong, R. D., Forrester, S., Cutler, J. N. & Paterson, D. (2006). *Soil Sci. Soc. Am. J.* **70**, 2038–2048.

McNulty, I., Paterson, D., Arko, J., Erdmann, M., Goetze, S. P. K., Ilinski, P., Krapf, N., Mooney, T., Retch, C. C., Stampfl, A. P. J., Vogt, S., Wang, Y. & Xu, S. (2003). *J. Phys. IV*, **104**, 11–15.

Medenwaldt, R. & Uggerhøj, E. (1998). *Rev. Sci. Instrum.* **69**, 2974–2977.

Meyer-Ilse, W., Denbeaux, G., Johnson, L., Bates, W., Lucero, A. & Anderson, E. (2000). *AIP Conf. Proc.* **507**, 129–134.

Mitrea, G., Thieme, J., Guttmann, P., Heim, S. & Gleber, S. (2008). *J. Synchrotron Rad.* **15**, 26–35.

Niemann, B., Guttmann, P., Rehbein, S. & Knöchel, C. (2003). *J. Phys. IV*, **104**, 273–276.

O'Day, P. A., Rivera, N., Root, R. & Carroll, S. A. (2004). *Am. Mineral.* **89**, 572–585.

Pohl, R. (1967). *Einführung in die Physik, 3. Teil – Optik und Atomphysik*, 12th ed. p. 180. Berlin: Springer.

Prietzel, J., Thieme, J., Eusterhues, K. & Eichert, D. (2007). *Eur. J. Soil Sci.* **58**, 1027–1041.

Prietzel, J., Thieme, J., Salome, M. & Knicker, H. (2007). *Soil Biol. Biochem.* **39**, 877–890.

Quiney, H. M., Peele, A. G., Cai, Z., Paterson, D. & Nugent, K. A. (2006). *Nat. Phys.* **2**, 101–104.

Schmahl, G. & Rudolph, D. (1969). *Optik*, **29**, 577–585.

Schneider, G., Denbeaux, G., Anderson, E. H., Bates, B., Pearson, A., Meyer, M. A., Zschech, E., Hambach, D. & Stach, E. A. (2002). *Appl. Phys. Lett.* **81**, 2535.

Schneider, G., Guttmann, P., Heim, S., Rehbein, S., Eichert, D. & Niemann, B. (2007). *AIP Conf. Proc.* **879**, 1291–1294.

Solomon, D., Lehmann, J., Lobe, I., Martinez, C. E., Tveitnes, S., Du Preez, C. C. & Amelung, W. (2005). *Eur. J. Soil. Sci.* **56**, 621–634.

Stöhr, J. (1992). *NEXAFS Spectroscopy.* Berlin: Springer Verlag.

Susini, J., Joyeux, D. & Polack, F. (2003). *J. Phys. IV*, **104**, V.
Susini, J., Salomé, M., Fayard, B., Ortega, R. & Kaulich, B. (2002). *Surf. Rev. Lett.* **9**, 203–211.
Sutton, S. R., Flynn, G., Rivers, M., Newville, M. & Eng, P. (2000). *Lunar Planet. Sci.* **31**, 1857.
Thieme, J., McNulty, I., Vogt, S. & Paterson, D. (2007). *Environ. Sci. Technol.* **41**, 6885–6889.
Thieme, J., Schneider, G. & Knoechel, C. (2003). *Micron*, **34**, 339–344.
Wang, Y., Jacobsen, C., Maser, J. & Osanna, A. (2000). *J. Microsc.* **197**, 80–93.
Warwick, T. *et al.* (1998). *Rev. Sci. Instrum.* **69**, 2964–2973.
Wiesemann, U., Thieme, J., Guttmann, P., Früke, R., Niemann, B., Rudolph, D. & Schmahl, G. (2001). *Nucl. Instrum. Methods Phys. Res. A*, **467–468**, 430–434.
Wiesemann, U., Thieme, J., Guttmann, P., Früke, R., Rehbein, S., Niemann, B., Rudolph, D. & Schmahl, G. (2003). *J. Phys. IV*, **104**, 95–98.
Wilhein, T., Kaulich, B., Di Fabrizio, E., Romanato, F., Cabrini, S. & Susini, J. (2001). *Appl. Phys. Lett.* **78**, 2082.
Wilke, M., Farges, F., Petit, P. E., Brown, G. E. & Martin, F. (2001). *Am. Mineral.* **86**, 714–730.
Wolter, H. (1952). *Ann. Phys.* **6**, 94–114.